Fourteenth USA/Europe Air Traffic Management Research and Development Seminar (ATM2021)

Robust CDO Trajectory Planning under Uncertainties in Weather Prediction

Shumpei Kamo, Judith Rosenow, Hartmut Fricke
Institute of Logistics and Aviation
Technische Universität Dresden
Dresden, Germany
{shumpei.kamo, judith.rosenow, hartmut.fricke}@tu-dresden.de

Manuel Soler
Department of Bioengineering and Aerospace Engineering
Universidad Carlos III de Madrid
Leganés, Spain
masolera@ing.uc3m.es

***Abstract*—Uncertainties are inherent in aircraft trajectory planning. Trajectories designed under deterministic hypotheses can cause significant performance degradation or constraint violation if the actual situation significantly differs from the assumed conditions. This study proposes computational strategies to plan a robust trajectory in terms of weather prediction, focusing on continuous descent operations. The members of the Global Ensemble Forecast System are used as a set of weather scenarios to reflect the nature of uncertainty in weather prediction along the flight execution. A robust optimal control problem is formalized, which simultaneously considers a set of trajectories for each of the weather scenarios while minimizing the expected value of the overall operational costs. Numerical simulations prove that the generated trajectories are robust for the predicted set of weather scenarios without violating the imposed constraints. Simulations with various cost index settings and preset required time of arrival further show that the proposed robust optimal control can cope with these varying operational settings.**

***Keywords*—Robust aircraft trajectory optimization, robust optimal control, global ensemble forecast system, continuous descent operations**

I. Introduction

Recent growing air traffic volume and resulting concerns of its environmental impact have motivated the authors to search for improved trajectory management strategies granting efficient and environmentally friendly missions. In particular, reduction of fuel burn, noise and gaseous emission are key performance indicators in the Europe's vision for aviation Flightpath 2050 [1] and the related research programmes by SESAR (Europe) [2], CARATS (Japan) [3] and NextGen (United States) [4]. In Europe, the European Union (EU) formulated the Single European Sky (SES) performance scheme to comply with the above expectations [5]. In these long-term plans, Continuous Climb / Descent Operations (CCO / CDO) are considered to be crucial components to contribute to these goals, enabling low to idle thrust settings by continuously descending, and avoiding level flight segments especially at low altitudes [6–8]. In 2018, Eurocontrol assessed the CDO's benefit pool for Europe and reported it in [9]. According to the report, 2017 traffic data showed that the average time in level flight from Top of Descent (ToD) performed by non-CDO flights were 217 seconds and the per-flight savings by potential CDO implementation were estimated to be 46 kg in fuel, 145 kg in CO_2 emission and 20 € in fuel costs. The report also estimated CDO can reduce noise emission by 1-5 dB per flight. Considering these benefit estimations, CDO and the Optimized Profile Descents (OPDs), the corresponding concept of NextGen, are listed in the roadmaps as one of the key measures to allow the Air Traffic Management (ATM) systems becoming more efficient and eco-friendly [2–4]. These more recent types of descent have been implemented in several regions across the world following these plans [10–12].

Trajectory optimization contributes to facilitating the CDO and maximizing its potential benefit. Studies on simulating and optimizing a descent trajectory, which eventually led to the CDO, have been carried out intensively in the last decade [11, 13, 14]. Necessity of re-optimizing the trajectory has also been raised in [15, 16] by examining deviation of the aircraft's energy state from the planned reference trajectory as a useful trigger for re-optimization. However, to the best of the authors' knowledge, these prior research works assumed deterministic scenarios and ignored impact of uncertainties. Yet, an optimal trajectory for a deterministic set of environmental conditions can lead to significantly higher costs than expected or can even become infeasible. Robust trajectory planning shall avoid these phenomena by providing a trajectory being compliant to unstable conditions.

Robust aircraft trajectory planning has recently become a field for intensive research and several applications for ATM have been proposed. González-Arribas et al. formalized a robust optimal control problem for cruise flight with uncertain wind situation by employing Ensemble Prediction Systems (EPS) [17] and confirmed the method could reduce the impact of uncertain wind on the planning, taking reference to one year of trajectory data and multiple origin-destination pairs [18]. This robust planning method was extended in [19] to the consideration of exposure to convection and cost-index based profiles. Franco et al. proposed a probabilistic trajectory predictor based on the probabilistic transformation method where they modeled a process to transform uncertainties from ground speed to estimated flight time and fuel burn

This work is a part of a project *Optimized CDO under Uncertain Environmental and Mission Conditions* funded by DFG, Deutsche Forschungsgemeinschaft (German Research Foundation) - project number: 327114631.

by convolution [20]. A different approach was followed by Legrand et al. [21], who solved the robust planning problem with dynamic programming. Recently, González-Arribas et al. proposed a heuristic method based on parallel Graphics Processing Unit (GPU) computation [22], finding robust trajectories in computational times that are compatible with real operations ($\sim$1 sec.) and considering not only the level flight, but including step-climbs and step-descents. These prior works have revealed importance of robust trajectory planning, however limited to the en-route phase of flight. To gain a comprehensive insight of how much robust planning is beneficial, attention should be paid to all flight phases. Especially, the descent phase holds potential for fuel burn reduction if CDO can be optimally executed as presented in [8]. Therefore, this study deals with robust trajectory planning to enhance capability and applicability of CDO to practical operation.

Considering the above, this study proposes computational strategies to plan a robust trajectory for CDO. We focus on in-flight trajectory planning carried out at flight deck and consider a pre-tactical planning horizon of at least 1-2 hours prior to reaching ToD. This research covers the trajectory optimization from cruise altitude down until reaching the Final Approach Fix (FAF). Weather prediction is taken as an uncertainty source and the members of the Global Ensemble Forecast System (GEFS) are used to reflect the nature of uncertainty in weather prediction along the flight execution.

The proposed trajectory planning is intended to be used for in-flight trajectory update triggered by significant change in weather prediction or assignment of a Controlled Time of Arrival (CTA) by Air Traffic Control (ATC). For a cruise trajectory, in-flight and mid-term planning has been investigated in [17, 23]. Important to note that unconsidered uncertainties can make the aircraft deviate from the planned trajectory at execution. It is out of scope for this study to investigate the impact of adhering to the planned trajectory or a tactical re-optimization strategies during execution. Some interesting studies on these topics can be found in [15, 16].

II. Models

A. Weather Models

Global Ensemble Forecast System (GEFS) is a set of weather forecast scenarios provided by the National Oceanic and Atmospheric Administration (NOAA) available online [24] and we utilize the version 11.0. GEFS consists of 21 separate weather forecasts called ensemble members. Each member is obtained by perturbing the initial conditions of the weather dynamics (known as the ensemble Kalman filter) to represent uncertainties in the model [25]. Small perturbations in the initial conditions evolve and lead to different weather states as time evolves. The forecasts are updated every 6 hours. Data are provided in a GRIdded Binary (GRIB2) format, where they are given at a position in the horizontal plane (specified by combination of latitude and longitude) and at a pressure level for at time of publication. The grid resolution is horizontally 1 $^\circ$ for the latitude and longitude, and vertically 100 hPa. More detailed investigation of the GEFS and its application to cruise-trajectory planning can be found in [23].

We utilize the GEFS data to obtain the ambient temperature, the pressure level and the wind speed vector along the estimated flight positions. The wind speed vector takes the horizontal components u and v, which are positive for the west-to-east wind flow and the south-to-north flow, respectively. GEFS does not contain the vertical wind component as it is usually one order of magnitude smaller than the horizontal component.

In order to apply the gridded GEFS data to the trajectory optimization problem, it is useful to increase the grid density by approximation. The simplest way is the linear interpolation connecting to each grid point. However, this method provides a function unable to be differentiated at any grid point, which is incompatible with the method we develop. As we discuss in III-C, we utilize the pseudospectral method, where the optimal control problem is transcribed into a Non-Linear Programming (NLP) problem and the discretized problem is numerically solved by the Sequential Quadratic Programming (SQP). The SQP requires the second derivatives of the models in the optimal control problem. Therefore, at least the second derivatives of the models must exist. To this end, we use second-order polynomial approximation, which is simple but guarantees a suitable mathematical function.

In the following, we follow two steps to derive the weather model: 1. interpolating the GEFS data and 2. finding the relationship between the pressure altitude and the geometric altitude. As for the second step, GEFS data and the flight dynamics (Equation of Motion: EoM) use different quantities to specify the vertical location: the former uses the pressure level pl while the latter uses the geometric altitude h above the Mean Sea Level (MSL) (Sec. II-B). In order to relate them, we need a transformation between pl and h.

For the first step: interpolation, we start it by limiting the 3D region for which to interpolate the data. The GEFS specifies the horizontal grid location with the longitude λ and the latitude ϕ, whereas the vertical location with the pressure level pl. With the hypotheses we make in Sec. II-B, where λ is fixed and ϕ strictly increases as time evolves, we can expect the following horizontal region to fly

$$\begin{aligned} \lambda &= \lambda_0 \\ \phi_0 \leq \quad \phi &\quad \leq \phi_f \end{aligned} \tag{1}$$

, where the subscripts 0 and f respectively denote the initial and final conditions of the optimal control problem (Sec. III-A). As for the vertical region, we expect

$$pl_{\text{low}} \leq pl \leq pl_{\text{up}} \tag{2}$$

, where we choose the lower and upper bounds pl_{low} and pl_{up} to cover the height from the FAF to the cruise level. We interpolate the GEFS data only for this region. Generally speaking, some difficulties occur when a region for modeling is too wide. For instance, if we try to capture phenomena in detail for a wide range, it inevitably requires high degree of polynomials, leading to unwanted oscillation. The limited region for approximation can make it possible to model details while avoiding use of high-degree polynomials.

We interpolate the GEFS data of the ambient temperature and the wind speed components for the limited region. Considering the computational costs, we adopted the second-order polynomials. Introduction of advanced approximation techniques, such as spline approximation, will be one of our future works. The polynomial approximation looks like:

$$y^{(s)}(\phi, pl) = \sum_{i,j=0}^{2} c_{y\ ij}^{(s)}\ \phi^i\ pl^j \tag{3}$$

, where $y^{(s)}$ is the approximation for the s-th member of GEFS and is either the temperature T or the wind speed components u, v. The polynomial coefficients $c_{y\ ij}^{(s)}$ are calculated by the least square method. The longitude λ is removed from (3) since we assume it is constant. A specific functional approximation is obtained for each ensemble member.

We then move to the second step: the transformation between pl and h. For this purpose, we utilize another data in GEFS: the geopotential height h_{gp}. This quantity is given in a grid format so it also can be expressed using (3):

$$h_{gp}^{(s)}(\phi, pl) = \sum_{i,j=0}^{2} c_{h_{gp}\ ij}^{(s)}\ \phi^i\ pl^j. \tag{4}$$

This study ignores the difference in the gravity dependency on latitude and altitude, and therefore assumes h and h_{gp} are identical. If we substitute $h_{gp}^{(s)}$ in (4) with $h^{(s)}$ and solve it in terms of pl, the pressure level can be obtained as:

$$pl = f_{pl}\left(h^{(s)},\ \phi\right). \tag{5}$$

f_{pl} is the function of $h^{(s)}$ and ϕ that is obtained when we solve the equality. (5) serves as a transformation law between h and pl and the aircraft altitude obtained from the EoM can be related to the pressure level. In this study, we adopt the second order polynomials for (3) so f_{pl} can be obtained as a closed form:

$$f_{pl} = \frac{-B - \sqrt{B^2 - 4AC}}{2A} \tag{6}$$

where

$$\begin{aligned} A &= c_{h_{gp}\ 02}^{(s)} + c_{h_{gp}\ 12}^{(s)}\phi + c_{h_{gp}\ 22}^{(s)}\phi^2 \\ B &= c_{h_{gp}\ 01}^{(s)} + c_{h_{gp}\ 11}^{(s)}\phi + c_{h_{gp}\ 21}^{(s)}\phi^2 \\ C &= -h^{(s)} + c_{h_{gp}\ 00}^{(s)} + c_{h_{gp}\ 10}^{(s)}\phi + c_{h_{gp}\ 20}^{(s)}\phi^2. \end{aligned} \tag{7}$$

Among the two solutions of (5), we take the one with the negative sign in front of the square root (6), as it produces reasonable value for pl. If we use higher-order polynomials, f_{pl} is obtained through numerical solution.

Applying (5) to (3), we eventually obtain the approximation $y^{(s)}$ as a function of ϕ and $h^{(s)}$:

$$y^{(s)}\left(\phi, h^{(s)}\right) = \sum_{i,j=0}^{2} c_{y\ ij}^{(s)}\ \phi^i\ f_{pl}^j\left(h^{(s)},\ \phi\right). \tag{8}$$

Three of the four quantities we are aiming to approximate, the ambient temperature T and the wind speed components u and v, are obtained by (8), while the other quantity, the pressure level, is approximated by (5). Another quantity required for trajectory calculation, the air density ρ, is obtained by the gas equation

$$\rho = \frac{pl}{RT}. \tag{9}$$

after approximating pl and T. Fig. 1 shows wind speed data of a member of GEFS and the corresponding approximation surface for an example.

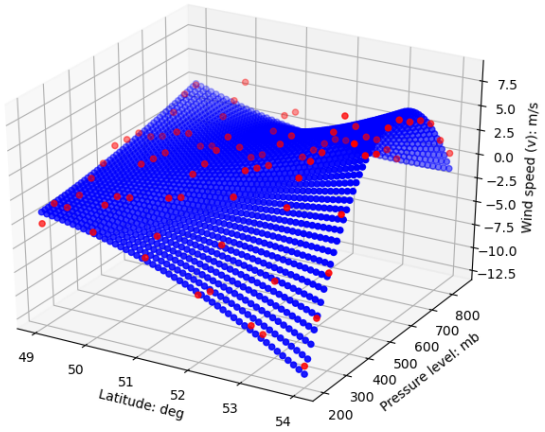

Figure 1: Approximation surface for the wind speed of a member of GEFS. Red dots are the data from GEFS and the blue surface is the approximation surface.

TABLE I. Relevant parameters of the WGS-84 Earth Model

Parameter	Notation	Value	Unit
Equatorial radius	a	6,378,137.0	m
Polar radius	b	6,356,752.3142	m
Reciprocal of flattening	$1/f$	298.257223563	
Eccentricity	e	0.081819190842622	

B. *Flight Performance Models*

In this study, we consider an aircraft as a dynamic system whose states are governed by a set of a point-mass EoM and are controlled through control inputs. We express the aircraft position in the geodetic coordinates (or the latitude-longitude-altitude coordinates) to align it with the grid expression of the weather model (Sec. II-A). We align our model with ISO 9300 or DIN 9300. We utilize the North-East-Down (NED) coordinates on the surface of the earth to describe the aircraft velocity [26], and the components of the wind speed model u and v are positive for the west-to-east wind flow and the south-to-north flow respectively. Details about deriving the EoM can be found in [26, 27]. We utilize the WGS-84 earth model defined by National Imagery and Mapping Agency (NIMA) [28], which [26] employs to derive the EoM in the geodetic coordinates. It is an ellipsoidal earth model characterized by the parameters listed in Table I.

We make five hypotheses when we model the aircraft's EoM. The first to third hypothesis is related to the aircraft. We assume the aircraft flies in the northern hemisphere exactly from the south to the north where the longitude is fixed, the azimuth is zero and the latitude strictly increases as time

evolves. Thus, the aircraft kinematics can be simplified and only the change of latitude ϕ and altitude h specifies the change of the aircraft position. The first hypothesis allows us to assume the bank angle always kept zero. The third hypothesis is that the change of the flight path angle is small enough to be kept zero $\dot{\gamma} \approx 0$. These three hypotheses result in ignoring the aircraft's lateral dynamics. They also lead to the equilibrium of the forces in the direction of lift as:

$$L = mg\cos\gamma - m\dot{v}\sin\gamma. \tag{10}$$

The lift force is calculated by (10) and the lift coefficient C_L by

$$C_L = \frac{2L}{\rho V^2 S} = \frac{2\left(mg\cos\gamma - m\dot{v}\sin\gamma\right)}{\rho V^2 S}. \tag{11}$$

The fourth and fifth hypotheses are for modeling the wind speed. The result of the above hypothesis, ignoring the aircraft's lateral dynamics, allows us to neglect the u component of the wind speed. For the fifth, we assume the weather forecast kept constant along the optimization. It means that the weather model II-A does not change over time but does change with only the aircraft position: latitude ϕ, longitude λ and altitude h. When we model the weather, we approximate the latest data available at the planning and assume it will not change during the execution.

With these hypotheses, the EoM for a point-mass aircraft is expressed as

$$\frac{d}{dt}\begin{Bmatrix} V \\ \phi \\ h \\ m \end{Bmatrix} = \begin{Bmatrix} \frac{F_T - D}{m} - g\sin\gamma - \frac{dv}{dt}\cos\gamma \\ \frac{V\cos\gamma + v}{R_\mu + h} \\ -V\sin\gamma \\ -FC \end{Bmatrix} \tag{12}$$

, where the true air speed (TAS) V, the latitude ϕ, the geometric altitude h and the aircraft's gross mass m form the aircraft state variables, whereas the thrust F_T, the flight path angle with respect to the air γ and the speed brake δ_{SB} are the control inputs to close the set of equations. We ignore the effect of the flap and slat controls on the aircraft dynamics. R_μ stands for the radius of curvature of the meridian's ellipse in the WGS-84 earth model and is given as a function of the latitude ϕ [26]:

$$R_\mu(\phi) = a\frac{1 - e^2}{(1 - e^2\sin^2\phi)^{3/2}}. \tag{13}$$

Parameters a and e are specified in Table I. The drag force D is modeled as:

$$D = \frac{1}{2}\rho V^2 S\left(C_{D_{\text{clean}}} + C_{D_{SB}}\ \delta_{SB}\right) \tag{14}$$

where $C_{D_{\text{clean}}}$ and $C_{D_{SB}}$ are taken from the Base of Aircraft Data family 4 (BADA4) [29]. D is a function of ϕ, V, h, m, γ and δ_{SB} as $C_{D\text{clean}}$ is a function of the Mach number $M = V/\sqrt{\kappa RT}$ and the lift coefficient (11), and all the weather quantities are functions of ϕ and h (Sec. II-A). The fuel consumption model

$$FC = C_{AC}\ pl\ T^{-1}\ C_F \tag{15}$$

is also taken from BADA4, where C_{AC} is a specific constant and the fuel coefficient C_F is a function of V, F_T and T:

$$C_F = C_F\left(V, F_T, T\right). \tag{16}$$

With the same discussion as we did for D, FC is a function of ϕ, V, h and F_T. We consider the change of the wind speed (dv/dt) in the TAS dynamics in (12). Detailed derivation of the wind speed gradient will be discussed later in this section.

So far, we have the time t as the independent variable for our formalization. From the optimal control viewpoint, this means t is required to be in the same domain $[t_0, t_f]$ for any of the state variables. As we see in Sec. III-C, we eventually aggregate the EoM to cover the dynamics for all the weather scenarios to create the robust optimal control problem. In the robust formalization, the necessity of t being in the same domain means the total flight time from the initial position to the FAF is fixed in every member of the trajectory ensemble. However, the authors are interested in variation in the total flight time due to uncertainties. Therefore, we stop having t as the independent variable. Instead, we treat the latitude ϕ, another variable which strictly increases as time evolves, as the new independent variable. It is reasonable to let ϕ in the same domain $[\phi_0, \phi_f]$ over the set of scenarios as the initial and final positions are fixed in the optimal control problem we consider. We perform this transformation of the independent variable by applying the chain rule

$$\frac{d}{dt} = \frac{d}{d\phi}\frac{d\phi}{dt} \tag{17}$$

to (12). $d\phi/dt$ is obtained from the second equation of (12). ϕ is now treated as the independent variable so it is removed from the left hand side of the EoM. Instead, t, which is now not considered as the independent variable, is regarded as a state variable and included in the EoM:

$$\frac{d}{d\phi}\begin{Bmatrix} V \\ t \\ h \\ m \end{Bmatrix} = \frac{R_\mu + h}{V\cos\gamma + v}\begin{Bmatrix} \frac{F_T - D}{m} - g\sin\gamma - \frac{dv}{dt}\cos\gamma \\ 1 \\ -V\sin\gamma \\ -FC \end{Bmatrix}. \tag{18}$$

We also need to calculate the time derivative in the first equation in (18). Since we ignore the time evolution of the weather while executing the optimal control process, the time derivative dv/dt is caused by the change of the aircraft position as

$$\frac{d}{dt}v(\phi, h) = \frac{\partial v}{\partial \phi}\frac{d\phi}{dt} + \frac{\partial v}{\partial h}\frac{dh}{dt} = \frac{\partial v}{\partial \phi}\frac{d\phi}{dt} + \frac{\partial v}{\partial h}\frac{dh}{d\phi}\frac{d\phi}{dt}. \tag{19}$$

Then, the corresponding part in (18) can be rewritten as

$$\begin{aligned} -\frac{R_\mu + h}{V\cos\gamma + v}\cdot\frac{dv}{dt}\cos\gamma &= -\frac{dt}{d\phi}\cdot\frac{dv}{dt}\cos\gamma \\ &= -\left(\frac{\partial v}{\partial \phi} + \frac{\partial v}{\partial h}\frac{dh}{d\phi}\right)\cos\gamma. \end{aligned} \tag{20}$$

In (20), $\partial v/\partial\phi$ and $\partial v/\partial h$ can be obtained by differentiating the wind speed approximation (8), whereas $dh/d\phi$ come from the third equation in (18).

For quick reference, Table II summarizes the major hypotheses we have made to derive the models.

TABLE II. Major hypotheses made in this study.

Weather	Aircraft
Time evolution ignored	South to north flight
Vertical wind ignored	Lateral dynamics ignored
u component ignored	γ dynamics ignored

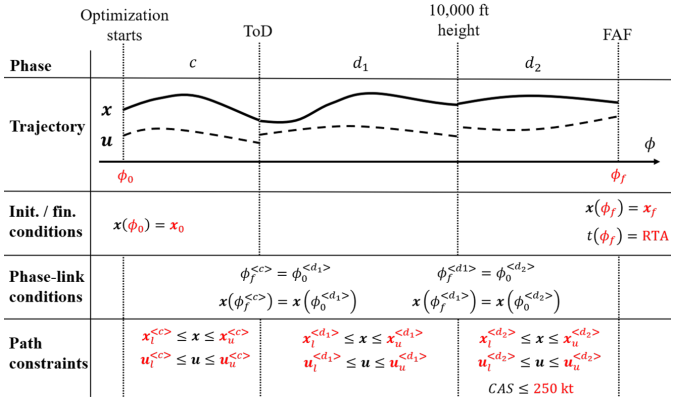

Figure 2: A sketch of the phases and the constraints in the deterministic multiple-phase optimal control problem. The symbols in red represent the given parameters.

III. Robust Descent Trajectory Planning

A. Deterministic Trajectory Planning as a Basis

We first formalize a deterministic trajectory optimization problem to form a basis of the robust optimization. It is carried out by applying the multiple-phase optimal control theory to the trajectory planning problem as the authors discussed in [30]. Overview of the phases and the corresponding constraints are shown in Fig. 2 for reference.

In the present study, we have three phases: the cruise (represented by c), the descent until 10,000 ft (d_1) and the further descent to FAF (d_2). In the c phase, the aircraft is to maintain the initial altitude but is allowed to change its speed. When it goes into the d_1 phase, it reduces its thrust to low level and leaves the cruise altitude. After passing 10,000 ft, the aircraft enters the d_2 phase lasting until the target FAF, where an additional constraint for the Calibrated Air Speed (CAS) is imposed.

In the optimal control problem, we have vector and scalar decision variables. The former are the state vector $\boldsymbol{x} = \{V, t, h, m\}^T$ and the control vector $\boldsymbol{u} = \{F_T, \gamma, \delta_{SB}\}^T$, whose components are functions of the independent variable ϕ. The latter are the initial latitudes $\phi_0^{<p>}$ and the final latitudes $\phi_f^{<p>}$ for each phase p. In the present study, we specify the initial and final latitudes of the whole phase:

$$\phi_0^{<c>} = \phi_0, \quad \phi_f^{<d_2>} = \phi_f. \tag{21}$$

Values of ϕ_0 and ϕ_f are listed in Sec. III. The present optimal control problem aims to determine these decision variables to minimize the objective functional.

The objective functional we consider includes the total operational costs consisting of the time-related costs and the fuel costs. The time costs are defined as the costs [€] charged for the flight time for the considered three phases represented by the final time $t(\phi_f)$. Linear relationship is assumed between the time costs and the final time through a coefficient C_t [€/s]: (Time costs) $= C_t\ t(\phi_f)$. The coefficient is modeled with the cost index $C_I = C_t/C_f$ [kg/s], where C_f denotes the current fuel price [€/kg]. Applying C_t to the time costs expression result in:

$$(\text{Time costs}) = C_I C_f\ t(\phi_f). \tag{22}$$

As for the fuel costs, they are defined as costs [€] charged for the fuel burn FB [kg] for the considered flight phases. The costs are assumed to be proportional to the fuel burn through the fuel price C_f. In Sec. II-B, we defined FC as the instant consumption of the fuel at a given time. Thus, FB is calculated as:

$$\begin{aligned} FB &= \int_{t_0}^{t_f} FC\, dt = \int_{\phi_0}^{\phi_f} FC \frac{dt}{d\phi} d\phi \\ &= \int_{\phi_0}^{\phi_f} FC \frac{R_\mu + h}{V\cos\gamma + v} d\phi = -\int_{\phi_0}^{\phi_f} \frac{dm}{d\phi} d\phi \\ &= m(\phi_0) - m(\phi_f) \end{aligned} \tag{23}$$

, where FC is transformed to the negative change of m using the fourth equation in (18). FB finally result in the difference between the initial mass and the final mass. Note that the initial mass $m(\phi_0)$ is specified as m_0 with the initial conditions we will discuss in (28). Consequently, the objective functional J is expressed as:

$$J = C_I C_f\ t(\phi_f) + C_f \{m_0 - m(\phi_f)\}. \tag{24}$$

The optimization problem has several constraints. First, the trajectory is governed by EoM (18). To facilitate the robust formalization in Sec. III-C, we call the components of the right hand side in (18) f_V, f_t, f_h, f_m, respectively and we define the dynamics vector $\boldsymbol{f} = \{f_V, f_t, f_h, f_m\}^T$. The dynamic constraints are expressed in a generic form as:

$$\frac{d\boldsymbol{x}}{d\phi} = \boldsymbol{f}(\boldsymbol{x}, \boldsymbol{u}, \phi). \tag{25}$$

We assume the dynamics $\boldsymbol{f}$ is unchanged throughout the considered phases.

The second type of constraints is the phase-link conditions. These are a set of equations that connects trajectories at the edge of successive phases. For the latitude as an independent variable, the end of the leading phase and the beginning of the following phase must be at the same latitude:

$$\phi_f^{<c>} = \phi_0^{<d_1>}, \quad \phi_f^{<d_1>} = \phi_0^{<d_2>}. \tag{26}$$

Combined with (21), the number of scalar decision variables for the present optimal control problem, which is originally six, is reduced to two. We take the final latitude for the first two phases $\phi_f^{<c>}$ and $\phi_f^{<d_1>}$ as the remaining decision variables. The same kind of phase-link conditions are also imposed on the state variables:

$$\boldsymbol{x}\left(\phi_f^{<c>}\right) = \boldsymbol{x}\left(\phi_0^{<d_1>}\right), \ \boldsymbol{x}\left(\phi_f^{<d_1>}\right) = \boldsymbol{x}\left(\phi_0^{<d_2>}\right) \tag{27}$$

These linkage conditions guarantee continuous connection between successive phases. It is important to note that this study does not impose these conditions on the control inputs

$\boldsymbol{u}$. This means we allow instant change of control at a phase edge.

The state vector $\boldsymbol{x}$ is also required to meet the initial and final conditions. The initial condition specifies the states at the very beginning:

$$\boldsymbol{x}(\phi_0) = \boldsymbol{x}_0. \tag{28}$$

$\boldsymbol{x}_0$ is a given vector from which the trajectory is generated. Unlike the initial conditions, the final conditions are basically only imposed on V and h:

$$\left\{ \begin{array}{c} V \\ h \end{array} \right\}(\phi_f) = \left\{ \begin{array}{c} V_f \\ h_f \end{array} \right\}. \tag{29}$$

For (28) and (29), $\boldsymbol{x}_0$, V_f and h_f are the given parameters and their values are in Table III. We also consider the Required Time of Arrival (RTA) at the FAF to evaluate how the CTA issued by the ATC affects the optimal trajectory. When the RTA (t_{RTA}) is imposed, the final state of t is constrained as:

$$t(\phi_f) = t_{\mathrm{RTA}}. \tag{30}$$

The rest of the constraints are the path constraints. For the phase p, they are expressed as:

$$\boldsymbol{x}_l^{<p>} \leq \boldsymbol{x}(\phi) \leq \boldsymbol{x}_u^{<p>}, \quad \boldsymbol{u}_l^{<p>} \leq \boldsymbol{u}(\phi) \leq \boldsymbol{u}_u^{<p>} \tag{31}$$

, where the subscripts l and u denote the lower and the upper bounds, respectively. All the bounds are given in Table IV. These constraints, imposed both on the states and controls, define the possible range for the variables to keep their values in. This prevents the trajectory from getting infeasible in terms of flight performance. In this sense, these constraints can also be called a "flight envelope", emphasizing the aerodynamic aspects. In addition to these path constraints, we also require the CAS to maintain slower than 250 kt in the d_2 phase (below 10,000 ft). Therefore, the following restriction is added for the latitude in $\phi_0^{<d_2>} \leq \phi \leq \phi_f$:

$$CAS(V, h, \phi) \leq 250\mathrm{kt}. \tag{32}$$

This constraint comes from the FAA regulation (14 CFR § 91.117) which bans flying faster than 250 kt (Indicate Air Speed: IAS) at 10,000 ft or lower. In (32), we regard CAS as a representative of IAS. Conversion law from TAS (V) to CAS is taken from BADA4 [29].

To summarize the discussion, the deterministic optimal control problem is formalized as: find the states $\boldsymbol{x}$ and controls $\boldsymbol{u}$ and the phase-edge latitudes $\phi_f^{<c>}, \phi_f^{<d_1>}$ to minimize the total operational costs (24) subject to the aircraft dynamics (25), the phase-link conditions (26), (27), initial and final conditions (28), (29), (30) and the path constraints (31), (32).

B. Definition of "Robustness"

Optimization in the presence of uncertainty has been studied intensively in the last decade both for static systems to seek the optimal values of the variables and also for dynamical systems to find the optimal control law as a function (optimal control). There are two different attitudes to deal with uncertainties in an optimization problem [31]. One is the stochastic optimization, where the Probability Density Functions (PDFs) of the targeted uncertainties are assumed to be known and introduced to the optimization problem. An example of stochastic optimal control applied to ATM can be seen in [32], where the stochastic optimization is applied to the aircraft conflict detection and resolution problem. Another is the robust optimization. Unlike the stochastic optimization, robust optimization does not assume the PDFs are known but instead it assumes sets of data representing the targeted PDFs, or so called the uncertainty sets [33]. The optimization problem is then formalized so that all the constraints are not violated for any realization of the uncertainty sets [31]. Application of the robust optimal control to ATM can be found in [17], where a cruise trajectory is optimized under wind speed uncertainties.

This study employs the robust optimal control to deal with the CDO trajectory planning under weather uncertainty. The reason for this is mainly due to the nature of GEFS data, where different sets of predicted weather situation are provided instead of PDFs.

In the development of robust optimization, several types of measure of robustness have been proposed [34]. The most common way of robustness measures is achieved by optimizing the problem for the worst case. This strategy picks up a scenario which makes the worst costs and optimizes the problem for it. Such costs are expressed with the Max function and thus this type of method is also called the Min-Max method. However, a solution optimized for the worst case, which usually happens rarely, is often too conservative for the rest of the cases and leaves room for improving the solution. To improve this issue, another definition of robustness has also been proposed. It regards a robust solution as the one that is optimized for the moments of the overall costs covering any realization of the uncertainty sets: such as the expected value (the first moment) or the variance (the second moment) or even higher [17].

This study employs the latter definition of robustness. We call a trajectory "a robustly optimized trajectory" when it is feasible for any predicted weather scenario given by GEFS and is optimized for the expected value of the costs covering all the scenarios. All the constraints are treated as hard constraints so that the optimal trajectory is flyable in any weather scenario, or resistant to changes of weather within the uncertainty range provided by GEFS data.

C. Robust Trajectory Planning

In this section, we formulate a robust optimal control problem for robust trajectory planning based on the deterministic formalization discussed in Sec. III-A. We assume a situation where the pilot and ATC are able to use the ensemble forecast from GEFS. We regard the members of GEFS as possible realizations of the uncertain weather during the flight they are planning. The 21 members of GEFS form a set of weather scenarios predicted to happen during the planned flight. To generalize the discussion, we use N_s as a number of weather scenarios. $N_s = 21$ for the GEFS version 11.0.

We first prepare the variables. We basically consider the aircraft states and control inputs that are different for a different weather scenario. So we explicitly express the state

and control vectors for the weather scenario s with the superscript $^{(s)}$ as $\boldsymbol{x}^{(s)}, \boldsymbol{u}^{(s)}$. On the other hand, the latitude ϕ as the independent variable stays common in a different scenario so it does not have the superscript $^{(s)}$. We apply the EoM (25) to each weather scenario s:

$$\frac{d\boldsymbol{x}^{(s)}}{d\phi} = \boldsymbol{f}\left(\boldsymbol{x}^{(s)}, \boldsymbol{u}^{(s)}, \phi\right). \tag{33}$$

Note that we assume the aircraft dynamics does not change in a different scenario, which is the same hypothesis for a different phase p, and therefore the dynamics vector $\boldsymbol{f} = \{f_V, f_t, f_h, f_m\}^T$ does not contain the superscript $^{(s)}$. Now we obtain a set of EoMs for N_s different weather scenarios. We call the set of trajectories generated from the set of EoMs "a trajectory ensemble". The trajectory for the weather scenario s is the s-th member of the trajectory ensemble. Then we aggregate the set of EoM as:

$$\frac{d}{d\phi}\begin{bmatrix} \boldsymbol{x}^{(1)} \\ \vdots \\ \boldsymbol{x}^{(N_s)} \end{bmatrix} = \begin{bmatrix} \boldsymbol{f}\left(\boldsymbol{x}^{(1)}, \boldsymbol{u}^{(1)}, \phi\right) \\ \vdots \\ \boldsymbol{f}\left(\boldsymbol{x}^{(N_s)}, \boldsymbol{u}^{(N_s)}, \phi\right) \end{bmatrix} \tag{34}$$

or more detailed expression as:

$$\frac{d}{d\phi}\begin{bmatrix} \begin{Bmatrix} V^{(1)} \\ t^{(1)} \\ h^{(1)} \\ m^{(1)} \end{Bmatrix} \\ \vdots \\ \begin{Bmatrix} V^{(N_s)} \\ \vdots \\ m^{(N_s)} \end{Bmatrix} \end{bmatrix} = \begin{bmatrix} \begin{Bmatrix} f_V\left(\boldsymbol{x}^{(1)}, \boldsymbol{u}^{(1)}, \phi\right) \\ f_t\left(\boldsymbol{x}^{(1)}, \boldsymbol{u}^{(1)}, \phi\right) \\ f_h\left(\boldsymbol{x}^{(1)}, \boldsymbol{u}^{(1)}, \phi\right) \\ f_m\left(\boldsymbol{x}^{(1)}, \boldsymbol{u}^{(1)}, \phi\right) \end{Bmatrix} \\ \vdots \\ \begin{Bmatrix} f_V\left(\boldsymbol{x}^{(N_s)}, \boldsymbol{u}^{(N_s)}, \phi\right) \\ \vdots \\ f_m\left(\boldsymbol{x}^{(N_s)}, \boldsymbol{u}^{(N_s)}, \phi\right) \end{Bmatrix} \end{bmatrix}. \tag{35}$$

If we define the aggregated state and control vectors as $\boldsymbol{X} = \left[\boldsymbol{x}^{(1)} \cdots \boldsymbol{x}^{(N_s)}\right]^T, \boldsymbol{U} = \left[\boldsymbol{u}^{(1)} \cdots \boldsymbol{u}^{(N_s)}\right]^T$, we can rewrite the aggregated set of equations with simpler expression:

$$\frac{d\boldsymbol{X}}{d\phi} = \boldsymbol{f}\left(\boldsymbol{X}, \boldsymbol{U}, \phi\right). \tag{36}$$

Next, we extend the other constraints. According to our definition of robustness (Sec. III-B), the solution must strictly satisfy all the imposed constraints under whatever weather scenario. It means that no deviation from the flight envelope is allowed. This mathematically stands for all the constrains being hard. Therefore, we impose exactly the same constraints for each scenario.

The phase-link conditions for ϕ are the same as (26). For $\boldsymbol{x}$ of the scenario s, they are:

$$\begin{aligned} \boldsymbol{x}^{(s)}\left(\phi_f^{<c>}\right) &= \boldsymbol{x}^{(s)}\left(\phi_0^{<d_1>}\right) \\ \boldsymbol{x}^{(s)}\left(\phi_f^{<d_1>}\right) &= \boldsymbol{x}^{(s)}\left(\phi_0^{<d_2>}\right). \end{aligned} \tag{37}$$

The initial and final conditions for the scenario s are

$$\boldsymbol{x}^{(s)}\left(\phi_0\right) = \boldsymbol{x}_0. \tag{38}$$

$$\begin{Bmatrix} V \\ h \end{Bmatrix}^{(s)}\left(\phi_f\right) = \begin{Bmatrix} V_f \\ h_f \end{Bmatrix}. \tag{39}$$

The right hand side of (38) and (39) do not contain the superscript (s) and therefore the common initial and final conditions are applied to each of the weather scenario. In terms of RTA, we require the mean arrival time at FAF to meet the time constraint:

$$\sum_{s=1}^{N_s} Pr^{(s)}\ t^{(s)}\left(\phi_f\right) = t_{\text{RTA}}. \tag{40}$$

$Pr^{(s)}$ denotes the probability for the weather scenario s to occur. In this study, we assume each GEFS member coming from perturbation in the initial condition is equally probable and $Pr^{(s)} = 1/N_s$ for all s. Then, (40) is re-written as

$$\frac{1}{N_s}\sum_{s=1}^{N_s} t^{(s)}\left(\phi_f\right) = t_{\text{RTA}}. \tag{41}$$

The path constraints for the phase p are

$$\boldsymbol{x}_l^{<p>} \le \boldsymbol{x}^{(s)}\left(\phi\right) \le \boldsymbol{x}_u^{<p>}, \quad \boldsymbol{u}_l^{<p>} \le \boldsymbol{u}^{(s)}\left(\phi\right) \le \boldsymbol{u}_u^{<p>} \tag{42}$$

, where the common lower and upper bounds are imposed for each weather scenario. The CAS limitation for the d_2 phase becomes:

$$CAS(V^{(s)}, h^{(s)}, \phi) \le 250\text{kt}. \tag{43}$$

In addition to these constraints coming from the deterministic optimal control problem, we introduce another type of constraints specific to the robust formalization. Considering that the planned trajectory is meant to be followed by the pilot or the FMS, we make the airspeed and the vertical trajectory common throughout the considered sets of weather scenarios. This is helpful as the pilot only needs to expect the unique profiles to follow with whatever scenario realized. To this end, we make V and h as unique variables for any of the weather scenarios. Together with the common independent variable latitude ϕ, h determines the unique vertical path. For the scenarios $2 \le s \le N_s$, the uniqueness constraints are:

$$V^{(s)}\left(\phi\right) = V^{(1)}\left(\phi\right), \quad h^{(s)}\left(\phi\right) = h^{(1)}\left(\phi\right). \tag{44}$$

, which require the trajectories to be identical to those for the scenario 1.

Lastly, we formalize the robust objective functional. According to our definition of robustness (Sec. III-B), the solution must give the minimum of the expected value of the total costs as:

$$\begin{aligned} J_{exp} &= E\left[(\text{total costs})\right] = \frac{1}{N_s}\sum_{s=1}^{N_s}(\text{total costs})^{(s)} \\ &= \frac{1}{N_s}\sum_{s=1}^{N_s} C_I C_f\ t^{(s)}\left(\phi_f\right) + C_f\left\{m_0 - m^{(s)}\left(\phi_f\right)\right\}. \end{aligned} \tag{45}$$

The initial mass m_0 is common over the trajectory ensemble whereas the final time $t^{(s)}\left(\phi_f\right)$ and mass $m^{(s)}\left(\phi_f\right)$ can have different values in a different ensemble member.

To summarize the discussion, the robust optimal control problem is to find the aggregated states $\boldsymbol{X}$ and controls $\boldsymbol{U}$ and the phase-edge latitudes $\phi_f^{<c>}, \phi_f^{<d_1>}$ to minimize the total operational costs (45) subject to the aggregated aircraft

TABLE III. Initial and final conditions. "Free" means the final condition is not imposed on the variable.

Variable		Initial	Final
ϕ	[deg]	50	53
V	[kt]	460	230
t	[s]	0	Free
h	[ft]	35,000	5,000
m	[kg]	63,700	Free

TABLE IV. Lower and upper bounds of the path constraints for each phase.

		c phase		d_1 phase		d_2 phase	
Variable		Low	Up	Low	Up	Low	Up
V	[kt]	230	470	230	470	230	470
t	[s]	0	3,000	0	3,000	0	3,000
h	[ft]	35,000	35,000	10,000	35,000	5,000	10,000
m	[kg]	54,200	63,700	54,200	63,700	54,200	63,700
F_T	[N]	0	123,000	0	12,300	0	12,300
γ	[°]	0.0	0.0	-5.0	0.0	-5.0	0.0
δ_{SB}	[-]	0.0	0.0	0.0	1.0	0.0	1.0

dynamics (36), the phase-link conditions (26), (37), the initial and final conditions (38), (39), (41), the path constraints (42), (43) and the uniqueness constraints (44).

The proposed optimal control problem is discretized by the Legendre-Gauss pseudospectral method. The resulting NLP problem is numerically solved by IPOPT [35], an open-source software package for large-scale nonlinear optimization and we utilize IPyOpt [36] as a Python interface for it. We have 20 pseudospectral nodes for each phase to balance the solution quality and the computing time.

IV. Numerical Simulation

We carried out series of numerical simulation to validate the proposed robust trajectory planning. We consider a scenario where a medium-range aircraft with 63,700 kg gross mass flies at constant altitude and at 4° longitude from 50° to 53° latitude (south-to-north flight), which covers basically the territory of Germany. The simulation starts at 50° (latitude) and at 460 kt (TAS), and maintains 35,000 ft. We assume the FAF is located at 53° latitude and at 5,000 ft altitude and the simulation is terminated if the aircraft reaches there. The distance to go between the initial aircraft position and the FAF is 182 NM. The TAS is required to be at 230 kt when arriving at the FAF. The initial and final conditions and the path constraint are set according to Table III and IV. The upper bound of TAS is set to be 10 kt higher than the initial TAS so that the aircraft can accelerate during the cruise phase. The maximum thrust of the aircraft is assumed to be 123000 N. In the d_1 and d_2 phases, small thrust (at most 10% of the maximum thrust) is allowed to be applied. We utilize the GEFS published on the 22nd of September 2020 at 0:00. We use a fuel price of 528.48 $/ton published by IATA [37] for 26 March 2021.

Fig. 3 shows the robust trajectories of the TAS V and the altitude h for the case where $C_I = 0$ without RTA imposed, and Fig. 4 depicts the histories of the corresponding control inputs: the thrust T, the path angle γ and the speed brake input δ_{SB}. The vertical lines show the phase edges. As seen in Fig. 3, the TAS and altitude trajectories are common for

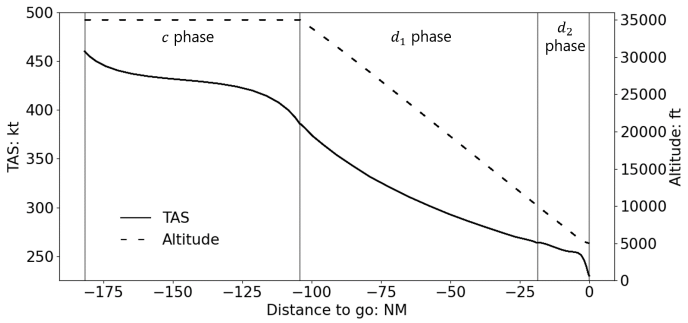

Figure 3: Robust trajectories of TAS and altitude ($C_I = 0$, RTA not imposed). Unique trajectories are calculated.

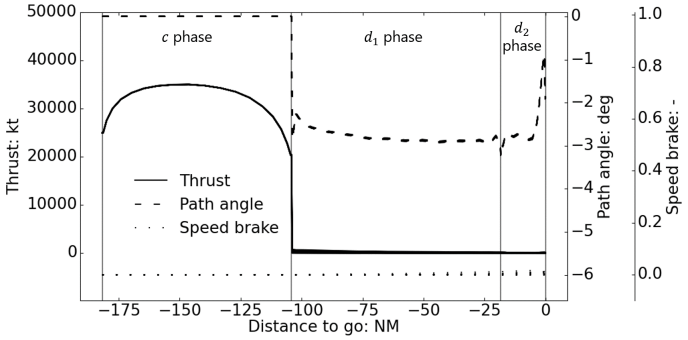

Figure 4: Robust trajectories of control inputs: thrust, flight path angle and speed brake ($C_I = 0$, RTA not imposed). Variation in trajectory appears over the 21 weather scenarios.

any of the 21 weather scenarios, reflecting the intention of (44). The aircraft decelerates while keeping its altitude in the c phase, and descends straightly down to the FAF in the d_1 and d_2 phase. At the very end of the d_2 phase, the aircraft reduces its TAS rapidly to meet its final condition at 230 kt. The ToD location is 104 NM to the FAF. As for the other state variables (t, m), the control variables (Fig. 4) and other relevant variables such as fuel burn, the trajectories are different for a different weather scenario. All the state and control variables meet the initial, final and path constraints for any weather scenario and thus this robust trajectory is always feasible. The average fuel burn for the considered phases is 549.6 kg and its standard deviation is 2.9 kg, while the average flight time is 1935 s and its standard deviation is 5.3 s. We call this trajectory a reference trajectory.

Fig. 5 shows the change of the robust TAS and altitude trajectories dependent on the cost index C_I, without RTA imposed. Trajectories with larger cost indexes have a longer cruise phase and consequently a steeper descent, and the overall speed is higher. The ToD location for $C_I = 80$ comes 24.3 NM later than that for $C_I = 0$. The flights with larger C_I, maintaining higher speed during the descent phase, briefly fly horizontally at the end of d_1 phase (starting at around 25 NM prior to the FAF) to rapidly reduce the airspeed so as to meet the CAS limitation for the d_2 phase (43). During these level flight segments, additional thrust is not used and thus additional fuel burn is not caused: just the exchange of the kinetic energy and the potential energy is performed. Fig. 6

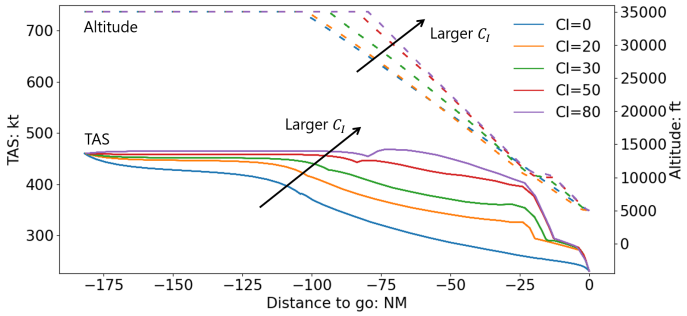

Figure 5: Change of the robust TAS and altitude trajectories dependent on the cost index C_I (RTA not imposed).

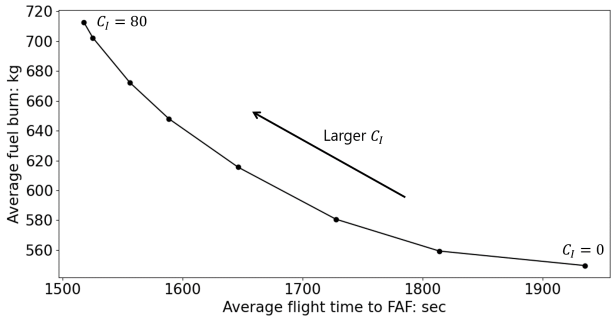

Figure 6: C_I-dependent relationship between the average flight time and the average fuel burn.

shows the C_I-dependent relationship between the average flight time and fuel burn of 21 weather scenarios from the initial aircraft position to the FAF. A larger C_I, putting more weight on the flight time in the objective functional (45), results in less fuel time instead of increased fuel burn. In the $C_I = 80$ case, 713 kg of fuel is burnt (30.0 % more than in the reference case) whereas the flight time was 1518 s (21.6 % less).

Fig. 7 depicts the change of the robust TAS and altitude trajectories dependent on the RTA, with $C_I = 0$, where the intervals of the selected RTAs are 60 s. As seen in the figure, a later RTA causes a longer cruise and lower overall speed. The ToD location for RTA $= 2050$ s comes 4.5 NM later than that for the reference trajectory without RTA imposed, whereas 0.5 NM earlier for RTA $= 1840$ s. Both the speed and altitude profiles look similar to those of the reference

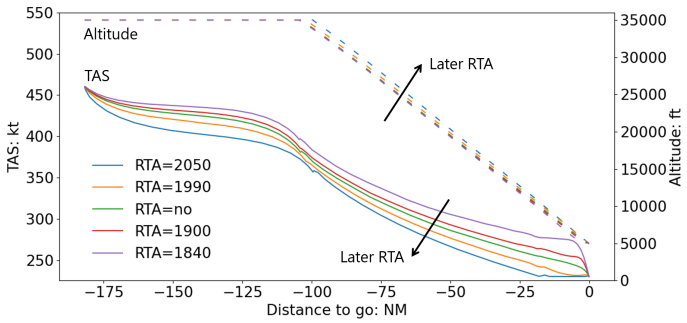

Figure 7: Change of the robust TAS and altitude trajectories dependent on the RTA ($C_I = 0$).

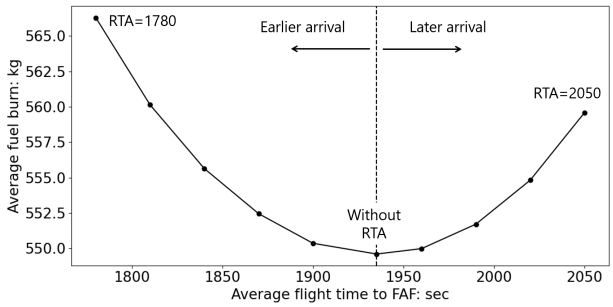

Figure 8: RTA-dependent relationship between the average flight time and the average fuel burn.

trajectory (Fig. 3), reflecting the objective of minimizing the fuel burn only. No level flight segment is found in the robust trajectories. Fig. 8 shows the relationship between the average flight time and fuel burn, changing with the RTA. The vertical line indicates the flight time of the reference trajectory and thus the aircraft in the cases to the right are required to arrive at the FAF later than the optimal time and vice versa. In the latest RTA$= 2050$ case where the flight time is required to be extended by 5.9 %, 559.6 kg of fuel is burnt which is 1.8 % more than in the reference case. In the earliest RTA$= 1780$ case with 8.0 % less flight time, the fuel burn is 566.3 kg (3.0 % more).

V. Conclusion

This study proposes computational strategies to plan a robust trajectory for CDO under uncertainties in weather prediction. The ensemble weather prediction of GEFS is utilized to create a set of weather scenarios and the data are interpolated using the second order polynomials. A deterministic multiple-phase optimal control problem is built to form a basis of the aimed robust optimal control problem, considering the longitudinal aircraft dynamics. We formalize a robust optimal control problem by aggregating the state and control variables as well as the aircraft dynamics for each of the weather scenario to create an aggregated EoM. In order to facilitate pilot's following of the robust trajectory, the TAS and altitude profiles are made common over the weather scenarios. Unlike conventional worst-case optimization, the proposed robust optimal control minimizes the expected value of the costs for the considered set of weather scenarios. Results of numerical simulation show that robust CDO trajectories with deterministic TAS and altitude can be obtained. They minimize the average operational costs without violating the imposed constraints, which meets the definition of robustness we define for this study. Simulation with different C_I and RTA shows the proposed robust optimal control can cope with these varying operational settings.

Our future works are mainly in two directions. First, we will extend the models further, including the 4D flight dynamics, advanced weather-data approximation (e.g. b-spline), more realistic speed brake model, time evolution of weather. Secondly, we will focus more on temporal uncertainties of a trajectory leading to loss of capacity and predictability. To address these issues, ATC's objectives will be introduced to

the robust optimal control problem, considering punctuality of flight. Methods will be developed to deal with a resulting multiple-objective optimal control problem.

REFERENCES

[1] "Flightpath 2050: Europe's vision for aviation," European Comission, Tech. Rep., 2011.

[2] "European ATM Master Plan 2020 edition," SESAR Joint Undertaking, Tech. Rep., 2019.

[3] "Long-term Vision for the Future Air Traffic Systems," Study Group for the Future Air Traffic Systems (MLIT), Tech. Rep., 2010.

[4] "NextGen implementation plan 2018-19," Federal Aviation Administration (FAA), Tech. Rep., 2018.

[5] "Single Europeam Sky performance scheme (EU regulation No 290/2013)," 2013.

[6] "Continuous descent operations (CDO) manual - Doc 9931," International Civil Aviation Organization (ICAO), Tech. Rep., 2010.

[7] "Continuous Climb and Descent Operations," European Organisation for the Safety of Air Navigation (Eurocontrol), Tech. Rep. [Online]. Available: https://www.eurocontrol.int/concept/continuous-climb-and-descent-operations

[8] H. Fricke, C. Seiß, and R. Herrmann, "Fuel and energy benchmark analysis of continuous descent operations," in *11th USA/Europe Air Traffic Management Research and Development Seminar (ATM Seminar 2015)*, 2015.

[9] "European CCO / CDO Action Plan," European Organisation for the Safety of Air Navigation (Eurocontrol), Tech. Rep., 2020.

[10] "Vertical flight efficiency at airports," European Organisation for the Safety of Air Navigation (Eurocontrol), Tech. Rep., 2020. [Online]. Available: https://ansperformance.eu/efficiency/vfe/

[11] D. Toratani, N. K. Wickramasinghe, and H. Hirabayashi, "Simulation techniques for arrival procedure design in continuous descent operation," in *2018 Winter Simulation Conference*, 2018, pp. 2249–2260.

[12] J. P. Clarke, J. Brooks, G. Nagle, A. Scacchioli, W. White, and S. R. Liu, "Optimized profile descent arrivals at Los Angeles international airport," Tech. Rep. 2, 2013.

[13] S. G. Park and J. P. Clarke, "Vertical trajecoty optimization for continuous descent arrival procedure," Tech. Rep., 2012.

[14] R. Dalmau and X. Prats, "Fuel and time savings by flying continuous cruise climbs estimating the benefit pools for maximum range operations," *Transportation Research Part D: Transport and Environment*, vol. 35, pp. 62–71, 2015.

[15] P. M. A. De Jong, "Continuous descent operations using energy principles," Ph.D. dissertation, Delft University of Technology, 2014.

[16] R. Dalmau and X. Prats, "Controlled time of arrival windows for already initiated energy-neutral continuous descent operations," *Transportation Research Part C: Emerging Technologies*, vol. 85, pp. 334–347, 2017.

[17] D. González-Arribas, M. Soler, and M. Sanjurjo-Rivo, "Robust aircraft trajectory planning under wind uncertainty using optimal control," *Journal of Guidance, Control, and Dynamics*, vol. 41, no. 3, pp. 673–688, 2018.

[18] J. García-Heras, M. Soler, and D. González-Arribas, "Characterization and enhancement of flight planning predictability under wind uncertainty," *International Journal of Aerospace Engineering*, vol. 2019, 2019.

[19] M. Soler, D. González-Arribas, M. Sanjurjo-Rivo, J. García-Heras, D. Sacher, U. Gelhardt, J. Lang, T. Hauf, and J. Simarro, "Influence of atmospheric uncertainty, convective indicators, and cost-index on the leveled aircraft trajectory optimization problem," *Transportation Research Part C: Emerging Technologies*, vol. 120, 2020.

[20] A. Franco, D. Rivas, and A. Valenzuela, "Probabilistic aircraft trajectory prediction in cruise flight considering ensemble wind forecasts," *Aerospace Science and Technology*, vol. 82-83, pp. 350–362, 2018.

[21] K. Legrand, S. Puechmorel, D. Delahaye, and Y. Zhu, "Feature article: Robust aircraft optimal trajectory in the presence of wind," *IEEE Aerospace and Electronic Systems Magazine*, vol. 33, no. 11, pp. 30–38, 2018.

[22] D. González-Arribas, E. Andrés-Enderiz, M. Soler, A. Jardines, and J. Garcıa-Heras, "Probabilistic 4D Flight Planning in Structured Airspaces through Parallelized Simulation on GPUs," in *International Conference for Research in Air Transportation (ICRAT) Conference*, 2020.

[23] M. Lindner, J. Rosenow, T. Zeh, and H. Fricke, "In-flight aircraft trajectory optimization within corridors defined by ensemble weather forecasts," Tech. Rep. 10, 2020.

[24] "Global Ensemble Forecast System (GEFS)," National Oceanic and Atmospheric Administration (NOAA), Tech. Rep., 1992. [Online]. Available: https://www.ncdc.noaa.gov/data-access/model-data/model-datasets/global-ensemble-forecast-system-gefs

[25] X. Zhou, Y. Zhu, D. Hou, and D. Kleist, "A comparison of perturbations from an ensemble transform and an ensemble kalman filter for the NCEP Global Ensemble Forecast System," Tech. Rep. 6, 2016.

[26] M. Peters and M. Konyak, "The engineering analysis and design of the aircraft dynamics model for the faa target generation facility," Tech. Rep. October, 2003.

[27] L. Weitz, "Derivation of a Point-Mass Aircraft Model used for Fast-Time Simulation," MITRE, Tech. Rep., 2015.

[28] "Department of Defense World Geodetic System 1984, Its Definition and Relationships With Local Geodetic Systems," National Imagery and Mapping Agency (NIMA), Tech. Rep., 1997.

[29] A. Nuic and V. Mouillet, "User manual for the base of aircraft data (BADA) family 4," European Organisation for the Safety of Air Navigation (Eurocontrol), Tech. Rep. 12/11/22-58, Version 1.3, 2016.

[30] S. Kamo, J. Rosenow, and H. Fricke, "CDO Sensitivity Analysis for Robust Trajectory Planning under Uncertain Weather Prediction," Tech. Rep., 2020.

[31] B. L. Gorissen, I. Yanikoğlu, and D. den Hertog, "A practical guide to robust optimization," Tech. Rep., 2015.

[32] Y. Matsuno, T. Tsuchiya, J. Wei, I. Hwang, and N. Matayoshi, "Stochastic optimal control for aircraft conflict resolution under wind uncertainty," *Aerospace Science and Technology*, vol. 43, pp. 77–88, 2015.

[33] X. Zhang, M. Kamgarpour, A. Georghiou, P. Goulart, and J. Lygeros, "Robust optimal control with adjustable uncertainty sets," Tech. Rep., 2017.

[34] H. G. Beyer and B. Sendhoff, "Robust optimization - A comprehensive survey," Tech. Rep. 33-34, 2007.

[35] A. Wächter and L. T. Biegler, "On the implementation of a primal-dual interior point filter line search algorithm for large-scale nonlinear programming," *Mathematical Programming*, vol. 106, no. 1, pp. 25–27, 2006.

[36] E. Xu, "IPyOpt - Python interface for the interior point optimzer COIN-OR IPOPT." [Online]. Available: https://gitlab.com/g-braeunlich/ipyopt

[37] "Jet Fuel Price Monitor," International Air Transport Association (IATA), Tech. Rep. [Online]. Available: https://www.iata.org/en/publications/economics/fuel-monitor/

AUTHOR BIOGRAPHY

Shumpei Kamo is a Ph.D. candidate and a research associate at Technische Universität Dresden. He studied aeronautics and astronautics at The University of Tokyo, Japan and received his bachelor and master degrees of engineering in 2015 and 2017, respectively. He joined TU Dresden in 2018 and is focusing on trajectory planning with uncertainties in the CDO-Speedbrakes project. His research interests include robust trajectory planning, multi-objective optimization and decision-making support.

Judith Rosenow studied Hydrology at Technische Universität Dresden from 2003 to 2008 where she specialized in Meteorology during her diploma thesis. In 2016 she finished her Ph.D. at Technische Universität Dresden with focus on optical properties of condensation trails aiming the possibility of optimizing a flight trajectory with respect to minimum climate impact of the generated contrail. Since 2014 she is a project leader of the projects MEFUL and ProfiFuel at Technische Universität Dresden.

Hartmut Fricke studied Aeronautics and Astronautics at Technische Universität (TU) Berlin where he received his doctor in ATM. In 2001 he finished his Habilitation on Integrated Collision Risk Modeling. Since December 2001, he is a professor for Aviation Technologies at TU Dresden and director of the Institute of Logistics and Aviation. In 2006 he was appointed Member of the Scientific Advisory Board to the German Federal Minister of Transport (BMVI). In 2012 he was elected scientific expert to DFG German Research Foundation. In 2013 he became SESAR External Expert, in 2020 member of the innovation board of the BMVI.

Manuel Soler received a Bachelor's and a Master's degree in Aeronautical and Aerospace Engineering from the Universidad Politcnica de Madrid. In 2013, he completed a Doctorate Degree in Aerospace Engineering from the Universidad Rey Juan Carlos. Since 2019, he is an Associate Professor with the Universidad Carlos III de Madrid, Getafe, Spain, where is the Director of the PhD Program in Aerospace Engineering. His research interests focus on optimal control, stochastic processes, meteorology, and climate change with application to Air Traffic Management (ATM). He is the coordinator of SESAR H2020 projects ALARM and START. He has been awarded with the SESAR Young Scientist Award in 2013 and the Luis Azcarraga Award by EnAire in 2016 and 2019.